AAS 15-615

ISOLATING BLOCKS AS COMPUTATIONAL TOOLS IN THE CIRCULAR RESTRICTED THREE-BODY PROBLEM

Rodney L. Anderson,* Robert W. Easton,† and Martin W. Lo*

Isolating blocks may be used as computational tools to search for the invariant manifolds of orbits and hyperbolic invariant sets associated with libration points while also giving additional insight into the dynamics of the flow in these regions. We use isolating blocks to investigate the dynamics of objects entering the Earth-Moon system in the circular restricted three-body problem with energies close to the energy of the L_2 libration point. Specifically, the stable and unstable manifolds of Lyapunov orbits and the hyperbolic invariant set around the libration points are obtained by numerically computing the way orbits exit from an isolating block in combination with a bisection method. Invariant spheres of solutions in the spatial problem may then be located using the resulting manifolds.

INTRODUCTION

It is well known from work by Conley, Easton, and McGehee that isolating blocks govern the behavior of transit orbits near the L_1 and L_2 libration points in the circular restricted three-body problem (CRTBP).[1,2,3,4] This knowledge has been used in general to aid in visualizing the flow in these regions and specifically to assist in particular analyses such as examining heteroclinic connections between periodic orbits in the CRTBP such as was done in Koon, Lo, Marsden, and Ross.[5] The L_2 gateway in particular is key for approach trajectories to a moon where multi-body effects are significant, a fact that was used in Anderson and Lo.[6,7] Ren and Shan[8] examined the boundary of orbits transiting through the gateway in a selected Poincaré section interior to the secondary using a bisection method, and focused on using transit orbits as targets for optimization. They also noted that some known invariant manifolds fell on this boundary. By making use of some of the fundamental characteristics of the isolating block, additional information and structures may be obtained. Specifically, the use of isolating blocks as a computational tool provides a means to both gain additional insight into the problem and compute the invariant manifolds of orbits and hyperbolic invariant sets associated with the libration points. The spatial CRTBP is used to model the dynamics of small masses in the Earth-Moon system, and this problem can be viewed as a three degree of freedom Hamiltonian system. The state space is six dimensional, and the manifolds of constant Jacobi energy have five dimensions. We investigate the dynamics of objects entering the Earth-Moon system with energies close to the energy of the L_2 Lagrange point (on the far side of the Moon). For the planar problem there are unstable periodic solutions near L_2, and the stable and unstable manifolds of these orbits guide the transition of orbits through the L_2 "bottleneck" formed when the Hills region opens up. For the spatial problem with fixed Jacobi energy, this bottleneck

*Member of Technical Staff, Jet Propulsion Laboratory, California Institute of Technology, 4800 Oak Grove Drive, M/S 301-121, Pasadena, CA 91109

†Professor Emeritus, Applied Mathematics, University of Colorado at Boulder, Boulder, CO 80309

contains a hyberbolic (unstable) invariant 3-sphere of solutions.[9,10] Stable and unstable manifolds of this invariant set guide the transit of orbits through the bottleneck just as in the planar problem.

Analytic methods for studying hyperbolic invariant sets in high dimensions are difficult to apply and are limited by issues of convergence in the normal form transformations[11,12] that are typically used. We introduce and use isolating blocks to locate invariant spheres of solutions and use a bisection method to numerically compute their stable and unstable manifolds. One virtue of the bisection method is that it requires relatively little analytic computation and can be implemented using numerical methods for solving ordinary differential equations. We choose arcs of initial conditions entering the block whose end points exit through disjoint exit sets. Every such arc must intersect the stable manifold of the trapped invariant set. Bisecting the arc and maintaining the end-point conditions leads to the accurate location of a point on the stable manifold. These points on the stable manifold may then be used to compute trajectories approaching the orbit or hyperbolic invariant set. Discarding an initial segment of an orbit on the stable manifold gives an approximation to its ω-limit set and therefore gives information about the dynamics restricted to the invariant set itself.

CIRCULAR RESTRICTED THREE-BODY PROBLEM EQUATIONS OF MOTION

A useful model for point mass or asteroid motion in the Earth-Moon system is the CRTBP in a rotating coordinate system with the Earth (or primary mass) located at position $E = (-\mu, 0, 0)$ and the Moon (or secondary mass) located at position $M = (\lambda, 0, 0)$ with $\lambda = 1 - \mu$. The mass parameter for the Earth-Moon system used here is $\mu = 1.2150584270571545 \times 10^{-2}$. The equations of motion for the point mass are these:

$$\begin{aligned} \ddot{x} &= \partial_x \Phi\,(x, y, z) - 2\dot{y} \\ \ddot{y} &= \partial_y \Phi\,(x, y, z) + 2\dot{x} \\ \ddot{z} &= \partial_z \Phi\,(x, y, z) \end{aligned} \tag{1}$$

where

$$\Phi\,(x, y, z) = \frac{1}{2}(x^2 + y^2) + U(x, y, z) \tag{2}$$

$$U\,(x, y, z) = \lambda/\rho_1\,(x, y, z) + \mu/\rho_2\,(x, y, z)\,. \tag{3}$$

The functions $\rho_1\,(x, y, z)$ and $\rho_2\,(x, y, z)$ are the distances from the asteroid to the Earth and Moon respectively.

It is sometimes convenient to use vector-matrix notation to represent these formulas. In that case, we use the notation $q = (x, y, z)'$. Treating E, M, q, and $\nabla\Phi\,(q)$ as column vectors, we set $\rho_1 = |E - q|$ and $\rho_2 = |M - q|$. The equations of motion then take the form

$$\ddot{q} = \nabla\Phi\,(q) + 2A\dot{q} \tag{4}$$

$$\nabla\Phi\,(q) = Fq + \lambda\,(E - q)\,{\rho_1}^{-3} + \mu\,(M - q)\,{\rho_2}^{-3} \tag{5}$$

$$A = \begin{pmatrix} 0 & -1 & 0 \\ 1 & 0 & 0 \\ 0 & 0 & 0 \end{pmatrix} \text{ and } F = \begin{pmatrix} 1 & 0 & 0 \\ 0 & 1 & 0 \\ 0 & 0 & 0 \end{pmatrix}. \tag{6}$$

The *Jacobi Integral* $J = \frac{1}{2}\,\langle \dot{q}, \dot{q} \rangle - \Phi(q)$ is a constant of motion for this model, and the *Jacobi constant* is defined by the equation $J = -C/2$. This is a convenient choice since then $\langle \dot{q}, \dot{q} \rangle =$

$2\Phi(q) - C$. For positive values of C the feasible values of q form the *Hill's Region*

$$m(C) = \{q : 2\Phi(q) - C \geq 0\} \tag{7}$$

The proof that the Jacobi integral is constant on solutions is easy in this notation:

$$\dot{J} = \langle \ddot{q}, \dot{q} \rangle - \langle \nabla\Phi(q), \dot{q} \rangle = \langle 2A\dot{q}, \dot{q} \rangle = 0. \tag{8}$$

The Euler-Lagrange equilibrium points for the equations of motion are found by setting $\ddot{q} = \dot{q} = 0$.

As a reference, the Jacobi constants computed at each libration point in the Earth-Moon system are

$$\begin{aligned} C_{L1} &= 3.1883411054012485 \\ C_{L2} &= 3.1721604503998044 \\ C_{L3} &= 3.0121471493422489 \\ C_{L4} &= C_{L5} = 2.9879970524275450. \end{aligned} \tag{9}$$

The Hill's regions will be important in defining the isolating block, and the regions corresponding to several of these Jacobi constants are given in Figure 1. See Pollard for a more detailed explanation of the CRTBP.[13]

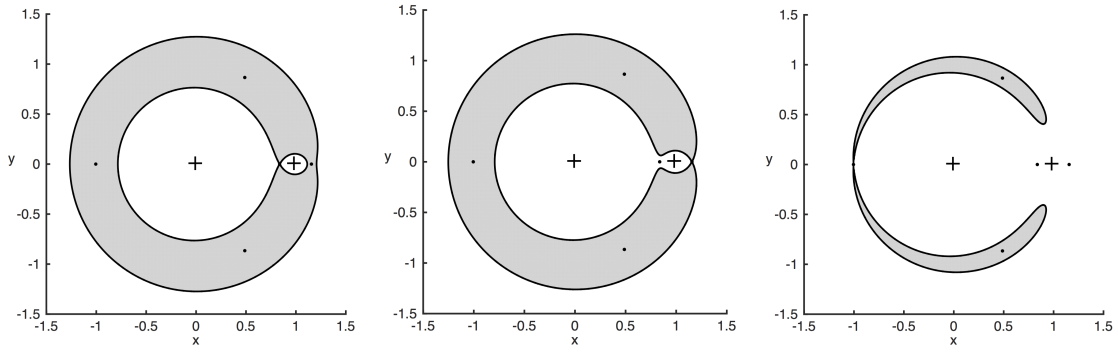

(a) C_{L1} (b) C_{L2} (c) C_{L3}

Figure 1. Hill's regions computed at the collinear libration point Jacobi constants in the Earth-Moon system.

COMPUTING INVARIANT MANIFOLDS USING ISOLATING BLOCKS

Isolating blocks have many theoretical uses in the study of dynamical systems.[10,14,15] However, their use as computational tools as discussed here may be new. The problem that suggests this use is the CRTBP in three space dimensions. Invariant three dimensional spheres of solutions are known to exist on five-dimensional energy surfaces with Jacobi constants close to those of the collinear Lagrange points. Later we will locate and investigate these spheres and their stable and unstable manifolds computationally.

For a smooth flow $\varphi(z,t)$ on a smooth manifold X contained in Euclidian space R^m, an *isolating block* is a compact subset B of X having continuous forward and backward exit time functions. The forward exit time function on B is defined by the formula

$$t^+(b) = \sup\{t : \varphi(b,s) \in B \text{ for } 0 \leq s \leq t\} \tag{10}$$

An infinite forward exit time is allowed. The backward exit time function is similarly defined. Exit time functions are defined on compact sets, but they are discontinuous in general. Suppose for some time $0 < \sigma < t^+(b)$ it happens that $\varphi(b, \sigma) \in \partial B$. This is called an "internal tangency," and initial points close to b may have exit times close to σ, and thus the exit time at b is discontinuous. If internal tangencies do not occur then the exit time functions are continuous.[2]

A useful condition that defines a block for a smooth flow on R^m is this: find a smooth real valued function V on R^m and a constant c such that $\{V \leq c\}$ is a compact manifold with boundary which is "convex to the flow." This means that orbits that are tangent to a point z on the boundary of B "bounce off," or more precisely, there exists $\delta > 0$ such that $\varphi(z, t)$ does not belong to B provided $0 < |t| < \delta$. The analytic condition that insures this is the condition is that when

$$V = c \text{ and } \dot{V} = 0, \text{ then } \ddot{V} > 0. \tag{11}$$

For a smooth map $\varphi(z)$ on R^m, the isolating block condition that B must satisfy is this: if three points z, $\varphi(z)$, $\varphi^2(z)$ belong to B, then $\varphi(z)$ is required to belong to the interior of B. (This is the discrete time version of no internal tangencies.) Define the forward exit time function and the exit set as follows:

$$t^+(b) = \sup\{m : \varphi^k(b) \in B \text{ for } 1 \leq k \leq m\} \tag{12}$$

$$Exit(B) = \{b \in B : t^+(b) = 1\} \tag{13}$$

Theorem: Suppose the exit set is the union of two non-empty subsets $Exit(B) = E_a \cup E_b$, and further that the sets $\varphi(E_a)$ and $\varphi(E_b)$ are a positive distance apart. Define the *exit route* for a point b with finite exit time to be exit through E_b if $\varphi^{(t^+(b))}(b) \in E_b$, and similarly define exit through E_a. Then there is a neighborhood of b in B whose points all have the same exit route.

Proof: If $b \in E_a$, then b has a neighborhood that exits, and the image of this neighborhood is far from the image of E_b (using continuity of the map φ). If the point b has exit time greater than 2, then all iterates of b up to the exit time must belong to the interior of B (from the definition of a block). Thus there is a neighborhood of b whose iterates stay close to the orbit of b and therefore all points in this neighborhood exit by the same route. If b has exit time 2, and $\varphi(b)$ belongs to the interior of B, then again a neighborhood of b has the same exit time and its points exit via the same route. In case $\varphi(b)$ belongs to the boundary of B, (and to E_a) then points near b that exit early by one step are close to $\varphi(b)$ and hence can not exit through E_b. Those that have the same exit time as b must have images near $\varphi(b)$ and hence can not exit through E_b. Again all points near b exit by the same route (through E_a).

Corollary: If C is a connected subset of B, and C contains a point that exits through E_a and also contains a point that exits through E_b, then C must contain a point having infinite exit time.

Proof: If all points of C exit, then the subsets of C that exit through E_a and that exit through E_b are disjoint open sets and their union is C. This is a contradiction because connected sets by definition are never the union of disjoint non-empty open sets.

This is the basis of our bisection algorithm for finding stable manifolds for hyperbolic invariant sets.

To illustrate the method we start with a simple example. The example is a map

$$\varphi : (x, y) \to (x', y') \tag{14}$$

of the plane defined by the equations

$$x' = 2x + \varepsilon a(x, y) \tag{15}$$

$$y' = y/2 + \varepsilon b(x, y) \tag{16}$$

For smooth functions a and b and sufficiently small ε, the compact region $B = \{|x| \leq 1, |y| \leq 1\}$ in the plane is an isolating block. The exit set is the subset E of B of points that φ maps outside of B. The exit set has two components E_{left} and E_{right} of points that exit to the left or to the right of B. Now consider the top boundary segment $C = \{|x| \leq 1, |y| = 1\}$ of B. The set C is connected, and its left and right endpoints exit left and right, respectively. We use the bisection method to search for a point of C that has infinite exit time. (This would be a point on the stable manifold of a saddle point in B under additional assumptions.) First, choose the midpoint of C. If this point has infinite exit time, the process is finished. If not, keep the sub-interval of C having endpoints that exit in opposite directions. Continue this process until the desired accuracy is obtained.

THE TOPOLOGY AND DYNAMICS OF A QUADRATIC HAMILTONIAN

To understand the geometry and dynamics near the L_2 point a standard approach is to linearize the dynamics by keeping only the quadratic terms of the Hamiltonian. We go a step further by constructing an example to show how topology and dynamics go together. An example of a Hamiltonian system with three degrees of freedom having hyperbolic invariant three-spheres uses the quadratic Hamiltonian

$$H(x, y) = \frac{1}{2}(y_1^2 + y_2^2 + y_3^2 + x_2^2 + x_3^2 - x_1^2) \tag{17}$$

Define $M(h) = \{(x, y) : H(x, y) = h\}$ which is a 5-dimensional manifold of constant energy. Then define $m(h) = \pi(M(h))$ where $\pi(x, y) = x$ is a projection of R^6 onto configuration space R^3.

The region $m(h)$ for $h > 0$ is a Hill's region, similar to the Hill's regions studied in the CRTBP. The Hill's region in configuration space is determined by the inequality

$$x_2^2 + x_3^2 \leq 2h + x_1^2 \tag{18}$$

This region is topologically equivalent to the Cartesian product of a line with a disk. The zero-velocity surface of the Hill's region is given by the condition

$$x_2^2 + x_3^2 = 2h + x_1^2 \tag{19}$$

For each point in the interior of $m(h)$ there is a 2-sphere of velocities

$$y_1^2 + y_2^2 + y_3^2 = 2h + x_1^2 - (x_2^2 + x_3^2) \tag{20}$$

such that the pair of points (x, y) belongs to the constant energy manifold $M(h)$. An intuitive way of thinking about the manifold $M(h)$ is that it is a "2-sphere bundle" over the Hill's region $m(h)$. The spheres collapse to points over the boundary of $m(h)$.

The equations of motion are decoupled and very simple for this example:

$$\begin{aligned} \dot{x}_1 &= y_1, \quad \dot{y}_1 = x_1 \\ \dot{x}_2 &= y_2, \quad \dot{y}_2 = -x_2 \\ \dot{x}_3 &= y_3, \quad \dot{y}_3 = -x_3 \end{aligned} \tag{21}$$

The first pair of equations gives a saddle in the (x_1, y_1) plane. The saddle has stable manifold given by the line $y_1 = -x_1$ and unstable manifold given by the line $y_1 = x_1$. The second and third pairs of equations have the phase portraits of centers.

The 4-dimensional plane $\{(x, y) : x_1 = y_1 = 0\}$ is invariant, and (for $h > 0$) the constant energy manifold $M(h)$ intersects this plane in an *invariant 3-sphere* S. The equations for S are

$$x_1 = y_1 = 0 \text{ and } y_2^2 + y_3^2 + x_2^2 + x_3^2 = 2h \tag{22}$$

The stable manifold of this sphere "projects" onto the stable manifold of the saddle point.

The stable and unstable manifolds of the saddle point $x_1 = y_1 = 0$ in the (x_1, y_1) plane are the crossed lines where $y_1^2 - x_1^2 = 0$. The stable manifold of S is then the set of points $W^s(S) = \{x_1 = -y_1 \text{ and } y_2^2 + y_3^2 + x_2^2 + x_3^2 = h\}$. This set is topologically the Cartesian product of S with a line. Similarly the unstable manifold of S has the same topology and is the set $W^u(S) = \{x_1 = y_1 \text{ and } y_2^2 + y_3^2 + x_2^2 + x_3^2 = h\}$.

Solutions starting in S lie on tori specified by allocating part of the total energy h to each oscillator. Such a torus is determined by the equations $x_2^2 + y_2^2 = b,\ x_3^2 + y_3^2 = h - b$. Also each such torus has its own stable and unstable manifolds.

The picture is basically the same when higher order terms are added to the Hamiltonian and the dynamics is non-linear. To prove this takes a considerable amount of analysis.[16]

The isolating block $B(h)$ (defined earlier in Equation 11) has the topology of the Cartesian product of an interval with a 4-sphere. The interval is the set $-a \leq x_1 \leq a$. The right boundary of the block projects onto a disk in configuration space. The disk is given by the inequality

$$2h + a_1^2 - (x_2^2 + x_3^2) \geq 0 \tag{23}$$

with $x_1 = a$. The boundary of this disk is contained in the zero-velocity surface of the Hill's region. Choosing a point (a, x_2, x_3) belonging to the interior of this disk, a 2-sphere S^2 of possible velocity vectors is compatible with keeping the energy h constant. The 2-sphere is given by

$$y_1^2 + y_2^2 + y_3^2 = 2h + a^2 - (x_2^2 + x_3^2) \tag{24}$$

The condition that the point $(a, x_2, x_3, y_1, y_2, y_3)$ belongs to the stable manifold of the 3-sphere is simple. The condition is $y_1 = -a$. Thus there is a circle of initial velocities in S^2 that give solutions on the stable manifold of the 3-sphere. With initial position (a, x_2, x_3), and initial velocity $(-a, y_2, y_3)$ belonging to S^2, the solution to the Hamiltonian equations is on the stable manifold.

Looking at the sphere S^2 by itself, initial velocities entering the block $B(h)$ through the right boundary must have $y_1 < 0$. All initial velocities in S^2 with $y_1 < -a$ give rise to transit orbits orbits which cross the block from right to left, and all initial velocities in S^2 with $0 > y_1 > -a$ give rise to non-transit orbits that enter and exit the block through the right boundary.

In preparation for constructing a block for the restricted problem one can define a function $V(x, y) = \frac{1}{2}x_1^2$ and show that $\ddot{V} > 0$ when $x_1 = a$ and $\dot{V} = 0$ and also that $\ddot{V} < 0$ when $x_1 = -a$ and $\dot{V} = 0$. Thus the block is "convex to the flow" in the sense that orbits that are tangent to the right boundary of the block (where $x_1 = a$) bounce off to the right and orbits tangent to the left boundary of the block bounce off to the left. This implies that the exit time for orbits starting in the block is continuous.[10,2]

Note that the stable manifold of S intersects the right boundary of the block in a 3-dimensional sphere. The equations of this intersection are these:

$$x_1 = a,\ y_1 = a\ ,\ y_2^2 + y_3^2 + x_2^2 + x_3^2 = h. \tag{25}$$

One could approximately find a point on this stable manifold by choosing an arc of initial conditions on the right boundary of the block with one endpoint exiting the block through the right boundary and the other endpoint exiting through the left boundary. This exercise could be used to test the accuracy of a numerical bisection method since the stable manifold is known in this situation.

CONSTRUCTING THE ISOLATING BLOCK NEAR L_2

We want to study the CRTBP flow near L_2 on the integral manifold $M\left(C\right)$ associated with Jacobi constant C. We will use the function $V\left(x,y,z,u,v,w\right) = (1/2)(x^2+y^2)$ to define an isolating block for the CRTBP flow near L_2. Define the set $B(r_1, r_2, C)$ by the conditions

$$\frac{1}{2}r_1^2 \leq V\left(x,y,z,u,v,w\right) \leq \frac{1}{2}{r_2}^2 \text{ and } J\left(x,y,z,u,v,w\right) = -\frac{1}{2}C. \tag{26}$$

To show that the set $B\left(r_1, r_2, C\right)$ is an isolating block for the flow on $M\left(C\right)$, it is sufficient to verify two "convexity" conditions:

$\ddot{V} > 0$ when $\dot{V} = 0$ on the outer boundary of B

$\ddot{V} < 0$ when $\dot{V} = 0$ on the inner boundary of B

We choose $r_1 = r^* - \delta$ and $r_2 = r^* + \delta$ for a small δ where the L_2 radius is $r^* \approx 1.1557$. We choose $C = C^* - \delta$ slightly below the Jacobi constant at the L_2 point $C^* = C_{L2}$. For small positive δ we will verify the convexity conditions.

The computation of $\ddot{V}$ for a general radius r may be completed as follows. Recall that we used the notation $q = (x, y, z)$. Thus

$$V = \left(\frac{1}{2}\right)\langle Fq, Fq\rangle = \left(\frac{1}{2}\right)r^2,\ \dot{V} = \langle Fq, F\dot{q}\rangle = 0,\ \ \ddot{V} = \ \langle F\dot{q}, F\dot{q}\rangle + \langle Fq, \ddot{q}\rangle \tag{27}$$

Now we use the equations of motion and the Jacobi integral:

$$\ddot{q} = Fq + \nabla\Phi\left(q\right) + 2A\dot{q} \tag{28}$$

$$\langle F\dot{q}, F\dot{q}\rangle = 2\Phi\left(q\right) - C - \dot{z}^2 \tag{29}$$

$$\langle Fq, \ddot{q}\rangle = \langle Fq, Fq\rangle + \langle Fq, \nabla(q)\rangle + \langle Fq, 2A\dot{q}\rangle \tag{30}$$

$$\langle Fq, Fq\rangle = r^2 \tag{31}$$

Then $\langle q, (E-q)\rangle = \rho_1\cos(\theta_1)|q|$ and $\langle q, (M-q)\rangle = \rho_2\cos(\theta_2)|q|$ where the angles are the angles between q and $E - q$, and between q and $M - q$.

$$\langle Fq, \nabla U\left(q\right)\rangle = \left[\lambda\rho_1^{-2}\cos\left(\theta_1\right) + \mu\,\rho_2^{-2}\cos\left(\theta_2\right)\right]|Fq| \tag{32}$$

$$\langle Fq, 2A\dot{q}\rangle = \langle Fq, 2AF\dot{q}\rangle = \pm 2\,|Fq|\,|F\dot{q}| = \pm 2r|F\dot{q}| \tag{33}$$

$$\ddot{V} = \langle F\dot{q}, F\dot{q}\rangle + \langle Fq, 2A\dot{q}\rangle + \langle Fq, Fq\rangle + \langle Fq, \nabla U(q)\rangle \tag{34}$$

$$\ddot{V} = \left(r \pm \sqrt{2\Phi - C - \dot{z}^2}\right)^2 - r\left[\lambda\rho_1^{-2}\cos(\theta_1) + \mu\,\rho_2^{-2}\cos(\theta_2)\right] \tag{35}$$

The next step is to determine where $\ddot{V} > 0$ when $r = r^* + \delta$ given a particular Jacobi constant. The first (positive) term in the expression for $\ddot{V}$ is minimized when $\dot{z} = 0$ and the negative sign is chosen. The first term is minimized and the second (negative) term is maximized when $z = 0$ because the Earth-asteroid and Moon-asteroid distances increase as the asteroid moves out of the xy plane. The second term is maximized when $q = r$. In this case $\theta_1 = \theta_2 = \pi$, and

$$\ddot{V} = (r-\gamma)^2 \; - r\left[\lambda\rho_1^{-2} + \mu\,\rho_2^{-2}\right] \tag{36}$$

$$\gamma = \sqrt{r^2 + 2[\lambda\rho_1^{-1} + \mu\,\rho_2^{-1}] - C} \tag{37}$$

It is difficult to see the behavior of $\ddot{V}(r, C)$ from the formula so numerical computations are used instead of analysis. As will be examined in more detail next, numerical explorations of the function $\ddot{V}(r, C)$ show that this function is positive for a (narrow) range of r-values at a selected Jacobi constant. Further explorations could demonstrate the limits to this construction. However our main purpose is to illustrate how the bisection method can be used to investigate the invariant set located inside a chosen isolating block.

SELECTING THE ISOLATING BLOCK BOUNDARIES FOR L_2

Numerically computing $\ddot{V}$ as a function of r and searching for locations where $\ddot{V} > 0$ provides a range of r values that may be used to define the outer radius of the cylinder used for the isolating block. In this case, trajectories approaching the boundary tangentially will "bounce" off the surface. $\ddot{V}$ as a function of x varies with C, and an appropriate radius may be selected for each C. A surface showing values of $\ddot{V}$ as a function of x and C is shown in Figure 2 along with a cross section for selected Jacobi constants at $C_{upper} = C_{L2} - \delta$, $C = 3.165$, and $C_{lower} \approx 3.1528$ where $\delta = 0.001$. It can be seen from the plot at $C = 3.165$ that a range of radius values will produce valid isolating blocks where $\ddot{V} > 0$, but larger radii will give $\ddot{V} < 0$. For $C = C_{upper}, 3.165,$ and C_{lower}, convenient radii are $r = 1.2, 1.2,$ and 1.315, respectively. The interior radius of the cylinder chosen for the isolating block may be selected anywhere on the other side of L_2 where $\ddot{V} < 0$, but it is important to locate it so that the invariant set is located within the isolating block. Practically, it is not difficult to locate this inner cylinder far enough toward the secondary that the invariant set is captured. The well-known planar Lyapunov orbit at this energy may also be used to insure that the inner radius is sufficiently small as the invariant set is expected to be bounded by the projected Lyapunov orbit in the xy plane.

IMPLEMENTING THE BISECTION METHOD IN THE PLANAR PROBLEM

Once the isolating block boundaries are selected, the transit and non-transit trajectories may be computed using a suitable grid along the boundary. For this analysis a grid of initial conditions on the outer cylinder was used to search for transit trajectories, and the initial conditions for the planar problem were specified by $q = f(C, \theta, \phi)$ where $\theta = \text{atan}(y/x)$ gives the initial position on the cylinder, and ϕ is used to specify the initial velocity direction as shown in Figure 3. Using this definition, $\phi = \pi$ travels directly inward toward the origin, and the considered ϕ values are $\pi/2 \leq \phi \leq 3\pi/2$. To search for transit trajectories, a grid of initial conditions across the cylinder

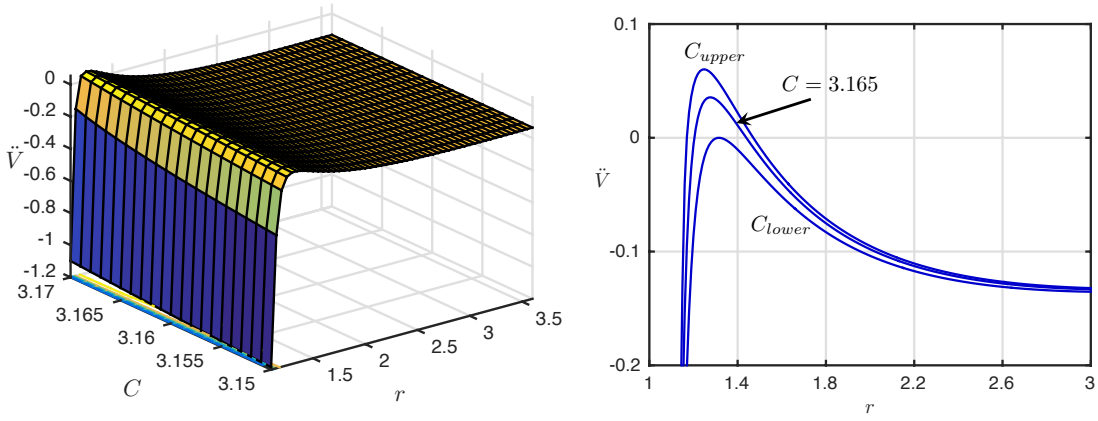

(a) $\ddot{V}$ over C and r (b)

Figure 2. $\ddot{V}$ across radii and C for cases where positive $\ddot{V}$ exists beyond L_2.

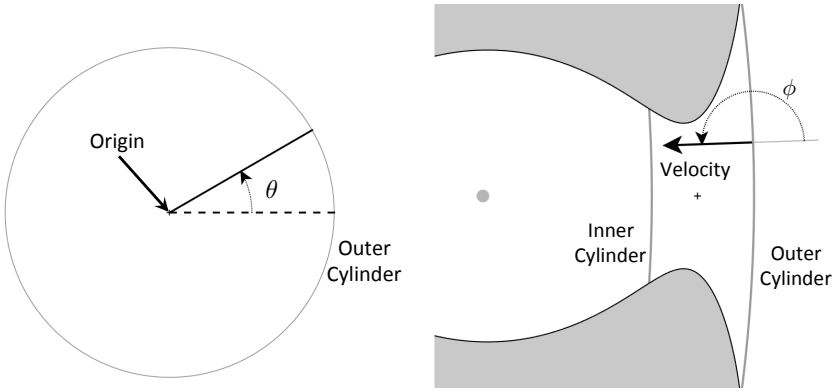

(a) (b)

Figure 3. Schematics illustrating the location of a grid point in configuration space (θ) and the direction of the velocity (ϕ).

and possible velocities are specified, and the trajectories are integrated forward in time. If any trajectories reach the inner cylinder, the time at which they cross may then be recorded. Practically, an upper boundary on the duration allowed for the integration must be selected, and it has been found that a duration of 20 dimensionless time units is sufficient to capture the desired trajectories in the Earth-Moon system.

The expected behavior of the trajectories computed across a subset of the grid is shown in Figure 4 for points located on the outer cylinder with a constant $\phi = -45$ deg. In this case the isolating block was chosen as $B(r_1, r_2, C) = B(1.12, 1.2, 3.165)$ which has the topology $I \times S^2$ as discussed in Easton.[2] At r_{inner}, it may be shown numerically that $\ddot{V} < 0$. These conditions result in trajectories that both transit through the isolating block exiting through the inner radius and those that exit through the outer radius. If the full grid is used those trajectories that cross r_{inner} may be computed, and the transit time may be plotted as a function of their initial conditions on the grid. Such a plot is computed for the C = 3.165 case in Figure 5. The set of trajectories that exit through r_{inner} form a disk spanning a significant region of the grid space shown in the figure, and the majority of

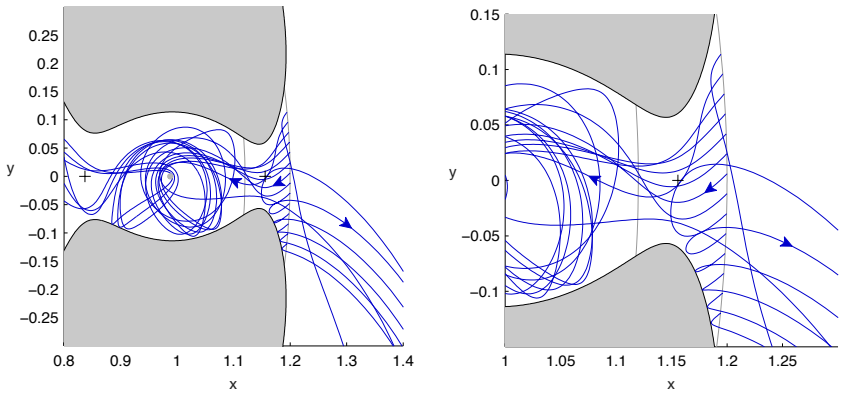

(a) (b)

Figure 4. Illustration of the trajectories on a subset of the grid with a constant ϕ of -45 deg. starting on the cylinder in the PCRTBP integrated forward for 20 dimensionless time units. The general expected behavior of the trajectories selected on the isolating block boundary may be observed here. Both transit and non-transit orbits may be observed with some traveling through the computed isolating block to reach the interior and others returning to the exterior region.

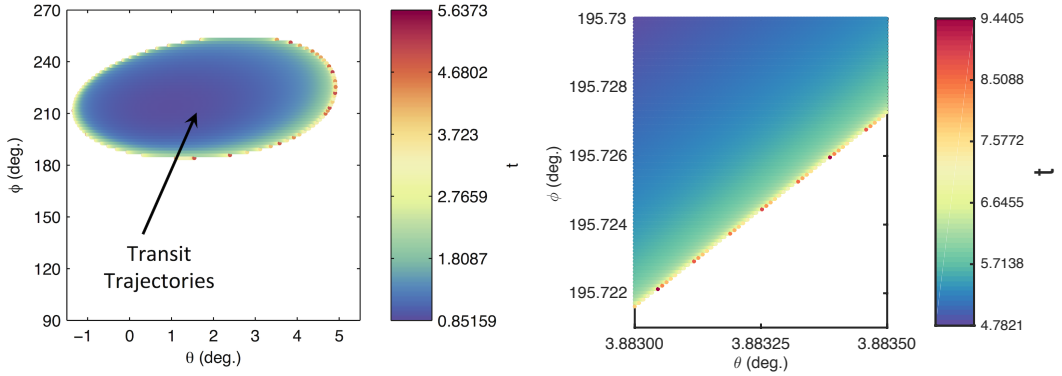

(a) Overview (b) Close View

Figure 5. Travel times for the transit trajectory corresponding to each point on the grid of initial conditions to reach r_{inner}. It is expected that the L_2 Lyapunov W^s trajectories will lie on the border of this region where the large transit times become large.

the trajectories exiting in this manner do so within a relatively short duration. It can be seen that trajectories near the border of this region of exiting trajectories require significantly more time to exit. Exploring a smaller region with a finer grid as shown in Figure 5(b), it can be seen that the exiting trajectories are continuous, and there is a distinct border to this region. The maximum time on the scale in Figure 5(b) is larger because a finer grid was used for this plot which captured more trajectories with higher exit time durations. The invariant manifolds of the L_2 invariant set in the planar case, or the planar Lypanov orbit, are found along this border. It is those trajectories that the bisection method will be used to compute.

Computing the Stable and Unstable Manifolds using the Bisection Method

As a first step in implementing the bisection method, the grid of initial conditions is searched to find the transit trajectories as shown in Figure 5(b). Once a boundary between transit and reflected trajectories was found, a bisection method was implemented to search for the boundary more precisely. The bisection method was considered converged when the computed change in initial conditions in radians for the next step was less than 1.0×10^{-14}. As the trajectories are integrated forward in time, the resulting trajectories lie on the stable manifold (W^s) of the L_2 Lyapunov orbit at the given energy. The converged trajectories and initial conditions on the cylinder are plotted for the Lyapunov L_2 W^s at C = 3.165 in Figure 6. The trajectories plotted in configuration space are

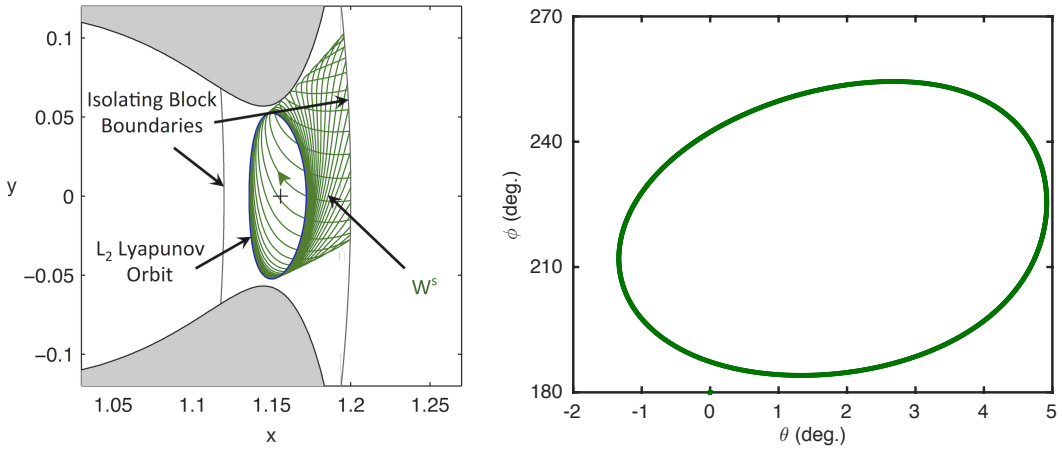

(a) Configuration Space Trajectories

(b) Converged Initial Conditions

Figure 6. Lyapunov L_2 W^s trajectories computed from $r = 1.2$ for C = 3.165. Each point in the initial conditions plot corresponds to a trajectory on the L_2 Lyapunov W^s, a subset of which are shown in the configuration space plot.

integrated until they cross $y = 0$ with $x < x_{L2}$ for the third time. The Lyapunov L_2 W^s may now be globalized by integrating the initial conditions on the cylinder backward in time. This method is in contrast to the usual method of computing the monodromy matrix from the variational equations and using an offset from the Lyapunov orbit to globalize the stable manifold. In particular, by using our bisection method, the periodic orbit and its invariant manifolds may be located without requiring earlier specific knowledge of the Lyapunov orbit. Examining the initial conditions in Figure 6(b) reveals that they form a curve in (θ, ϕ). This may be expected because the Lyapunov orbit is one-dimensional (S^1), and the stable manifold is a cylinder or $S^1 \times R^1$. When the stable manifold intersects the outer radius of the isolating block it does so in an arc in configuration space with a corresponding arc of velocities. The resulting curve is a one-sphere in θ and ϕ.

While the stable manifold is computed by integrating forward in time, the corresponding unstable manifold (W^u) may be computed by reversing the time and the initial direction of the velocity along the grid. Those trajectories traveling backward in time to the L_2 invariant set may then be computed using a bisection method. The trajectories resulting from this process on the Lyapunov L_2 W^u are shown in Figure 7. The curve of initial conditions mirrors that of the initial conditions for the stable manifold case as would be expected from the symmetry about the $y = 0$ line in the CRTBP. Similar results are obtained when the method is applied to the computation of the stable and unstable manifolds of the hyperbolic invariant set in the spatial problem.

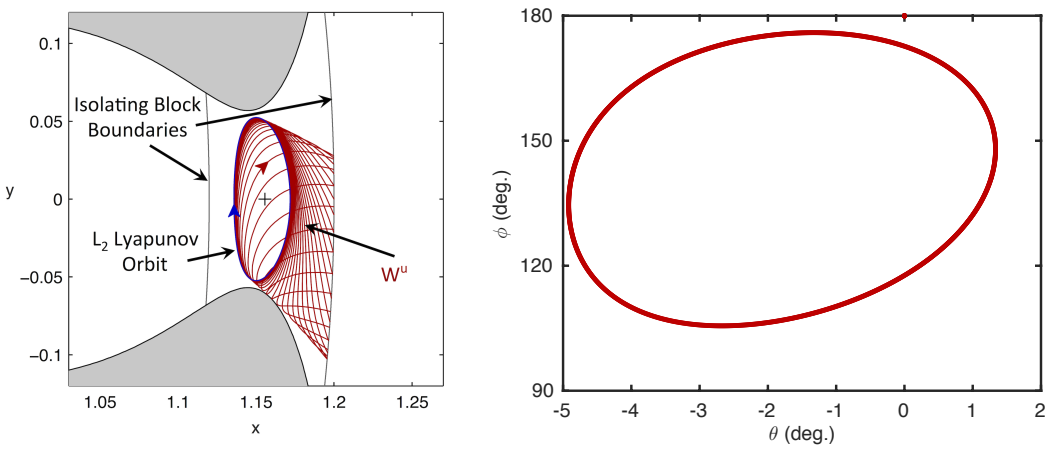

(a) Configuration Space Trajectories

(b) Converged Initial Conditions

Figure 7. Unstable manifold trajectories computed from $r = 1.2$ for C = 3.165. Each point in the initial conditions plot corresponds to a trajectory on the L_2 Lyapunov W^u, a subset of which are shown in the configuration space plot.

IMPLEMENTING THE BISECTION METHOD IN THE NON-PLANAR PROBLEM

While the application of the bisection method to find the L_2 invariant set in the non-planar problem is conceptually similar to the planar case, the additional dimension requires several modifications to both the computational algorithm and the visualization. Briefly, for this case we fix an initial point q in configuration space and choose a velocity such that the pair (q, v) belongs to the integral manifold $M(C)$. Then we use the pair (q, v) as an initial condition and run the numerical solution forward in time. The isolating block boundaries are three-dimensional cylinders centered on the origin, and the grid of initial conditions for multiple locations in configuration space q lies on this cylinder. Rather than using angles to parameterize the velocity, a grid of $\dot{y}$ and $\dot{z}$ is chosen. Then,

$$\dot{x} = \pm\sqrt{x^2 + y^2 + 2\frac{1-\mu}{\rho_1} + 2\frac{\mu}{\rho_2} - C - \dot{y}^2 - \dot{z}^2}, \tag{38}$$

and the selected initial $\dot{x} < 0$.

Transit Trajectories

A plot of transit trajectory times similar to that generated for the planar case may be computed in the spatial case. Given the extra dimension of the problem, the plot is generated for a specific q on the cylinder. The same isolating block $B(1.12, 1.2, 3.165)$ is selected for an illustrative case. The location on the cylinder in configuration space for this case is specified by $\theta = 0.75$ deg. and $z = 0.01$. The trajectories are integrated for $\Delta t = 20$, and the time required to reach a cylinder with r_{inner} is recorded if the trajectory reaches the cylinder within the given Δt. The resulting initial conditions that produce transiting orbits are plotted in Figure 8. A subset of the transit orbits are shown in configuration space in Figure 9. The general characteristics of the transit orbits for this particular point on the grid may be observed from the plots. Note that some of the structure observed in the trajectories is a result of the rougher grid used to generate these plots.

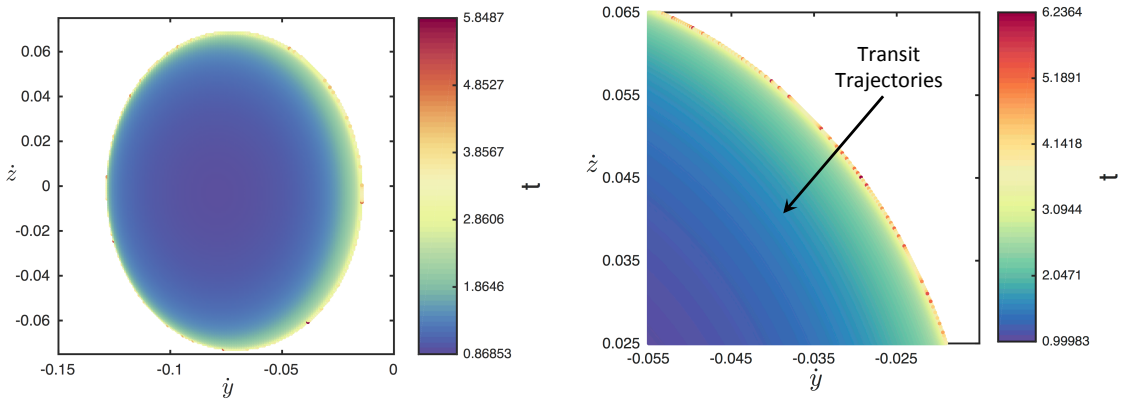

(a) Overview (b) Close view

Figure 8. Transit trajectory times as a function of the initial conditions in $\dot{y}$ and $\dot{z}$. For this case, $\theta = 0.75$ deg., $z = 0.01$, and C = 3.165 with $r_{outer} = 1.2$ and $r_{inner} = 1.12$.

Stable Manifold Computation

A bisection method similar to the one used for the planar case may be employed to compute the stable manifold of the invariant 3-sphere at L_2 in the spatial case. The computation and visualization of the resulting trajectories becomes more difficult in this case because the trajectories will intersect the cylinder at multiple points in configuration space with a range of velocities associated with each position. The visualization of the W^s trajectories that project onto a particular point in configuration space becomes more tenable though, so the computation of W^s trajectories using the bisection method is demonstrated here first by applying it to the case corresponding to Figure 8. In this case, for the selected point on the cylinder in configuration space, a grid of $\dot{y}$ and $\dot{z}$ was selected so that it contained the transit trajectories computed earlier. Again, $|\dot{x}|$ was chosen so that C = 3.165 with $\dot{x} < 0$. Applying the bisection method across $\dot{y}$ and $\dot{z}$ converged on the initial conditions shown in Figure 10. Each point in Figure 10 represents a trajectory approaching the invariant set located around L_2. Recalling the quadratic Hamiltonian example gives some additional insight into the results found here. As discussed there, for a particular point in configuration space a 2-sphere of possible velocities exists at a particular energy. There is then a circle of initial velocities in S^2 that gives solutions on the invariant 3-sphere W^s, which is what we see in Figure 10.

A selected set of these trajectories is shown relative to the Hill's region in Figure 11. Each of these trajectories asymptotically approaches the invariant 3-sphere, but numerically they will eventually wander away from the invariant 3-sphere and leave the vicinity of L_2. Practically speaking, this typically happens within three to four revolutions of the trajectory around L_2, and the integration of each of these trajectories is stopped after this many revolutions to capture the trajectories as they are asymptotically approaching the invariant ω-limit set. Note that some of the structure is again related to the grid used to compute a subset of the trajectories. From these plots it is apparent that the individual trajectories may be approaching quasiperiodic orbits as would be expected for trajectories approaching the invariant set in the quadratic Hamiltonian problem. The type of motion that each of these trajectories approaches asymptotically may be more clearly seen by plotting some of the trajectories separately as is done in Figure 12. In these plots, it can be seen that some of the trajectories stay very close to the plane, while others vary significantly in the z direction. Each

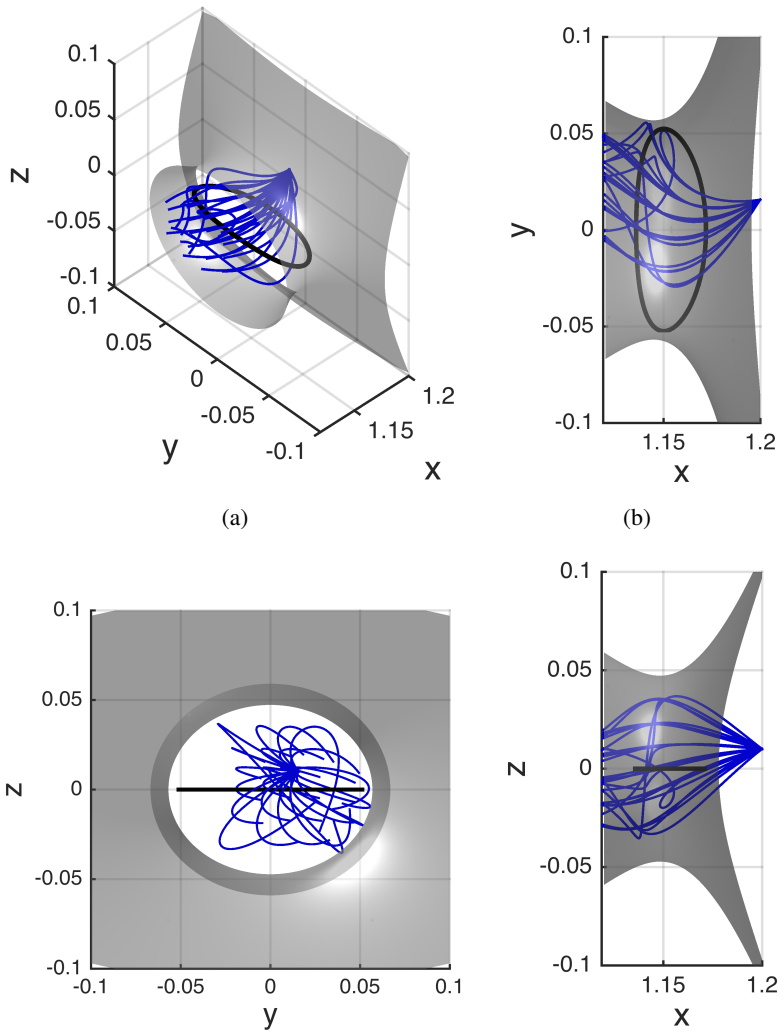

Figure 9. Sample of trajectories in configuration space corresponding to Figure 8. A Lyapunov orbit is plotted at the same energy level as the transit orbits along with the spatial Hill's region boundary for reference.

trajectory for these cases does appear to have a quasiperiodic motion, although the trajectory in Figure 12(a) is closer to periodic.

These tractories are only a small subset of the trajectories on the invariant 3-sphere W^s that may be computed, and some additional features may be observed by plotting additional trajectories. Larger sets of the trajectories on W^s are shown in configuration space in Figure 13. In each case, the additional trajectories fill in the space near the original trajectories. It is more difficult to observe each trajectory, but the variety of motion may be observed.

The W^s trajectories computed so far approach the invariant 3-sphere asymptotically, so it is possible to trim the initial portion of the trajectory to only capture the asymptotic approach. The asymptotic portion gives an approximation to the invariant ω-limit set of the trajectory inside the in-

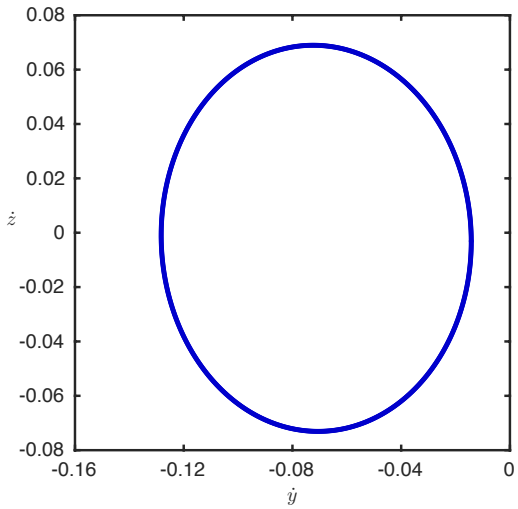

Figure 10. Converged initial conditions on W^s of the invariant 3-sphere at the point in configuration space chosen in Figure 8. Each point in the plot corresponds to a trajectory on W^s approaching the invariant 3-sphere.

variant 3-sphere at L_2. Performing this procedure produces the trajectories shown in Figure 14. The quasiperiodic nature of the trajectories may be more easily observed here. Again, both trajectories near the plane and with a significant vertical component are observed.

The trajectories computed on the invariant 3-sphere W^s so far have all been computed for a single point in configuration space located on the cylinder. These trajectories provide a general indication of the characteristics of W^s, but a more complete picture of the W^s may be obtained by varying the position on the cylinder used to compute the trajectories in configuration space. Varying one of the components on the cylinder, such as z, also shows how the W^s trajectories vary as the edge of the disk of transit trajectories in configuration space is approached. Such a plot for fixed x and y with varying z is shown in Figure 15. The converged initial conditions on the invariant 3-sphere W^s are shown in the center plot for selected values of z as labeled. As can be seen from the plot, for each value of z, the initial conditions form a circle, as seen for the $z = 0.01$ case. As the boundary of the transit trajectories in configuration space is approached (at higher z values), the circle converges to a point. The upper value of z for the boundary of the transit trajectory disk in configuration space was chosen using another bisection method in z, and it lies very close to the edge where the computed trajectories at this point are all very similar. The corresponding converged trajectories for each z point are shown on the sides of the figure as labeled. It can be seen that for low z values (near the center of the disk in configuration space), the trajectories have a large range of types of motion. As z increases, the trajectories become more similar, and the range of types of motion is reduced. Taken together, these trajectories provide a more complete picture of the characteristics of the invariant 3-sphere.

By varying the initial conditions in configuration space, the border of the initial conditions in this configuration space that produce trajectories on the stable manifold of the invariant 3-sphere may be determined. Using a bisection method in the z direction allows us to find this border in configuration space as shown in Figure 16. Topologically, the computed region forms a disk on the isolating block boundary cylinder. In this figure, the dark edge represents those locations where a single trajectory approaches the invariant 3-sphere, and the interior of the disk contains those points where circles

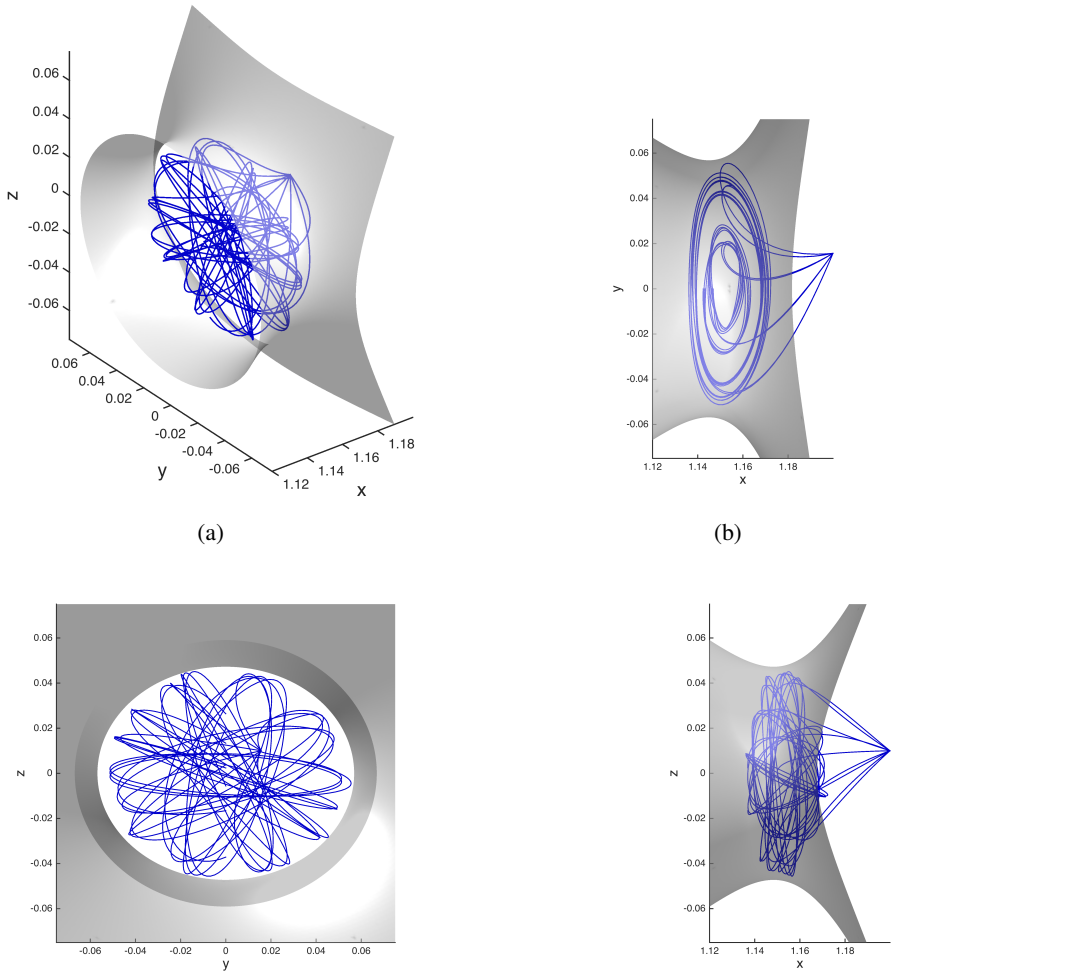

Figure 11. Selected trajectories on W^s of the invariant 3-sphere at C = 3.165 for the point on the cylinder at $\theta = 0.75$ deg. and $z = 0.01$.

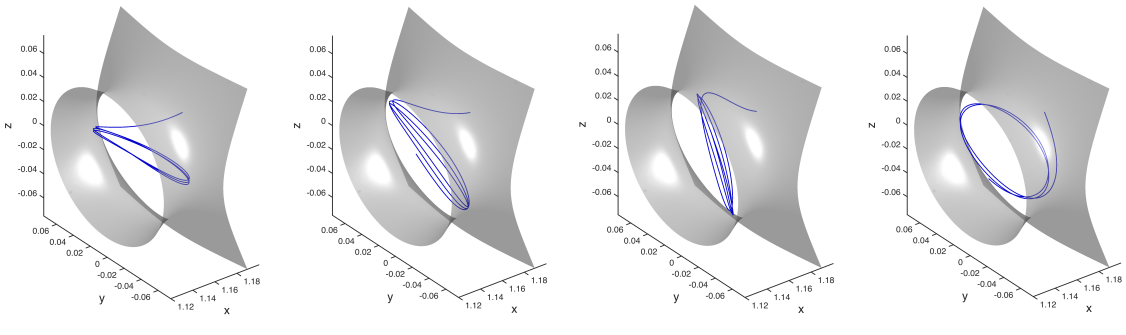

Figure 12. Selected trajectories on W^s of the invariant 3-sphere plotted separately at C = 3.165 for the point on the cylinder at $\theta = 0.75$ deg. and $z = 0.01$.

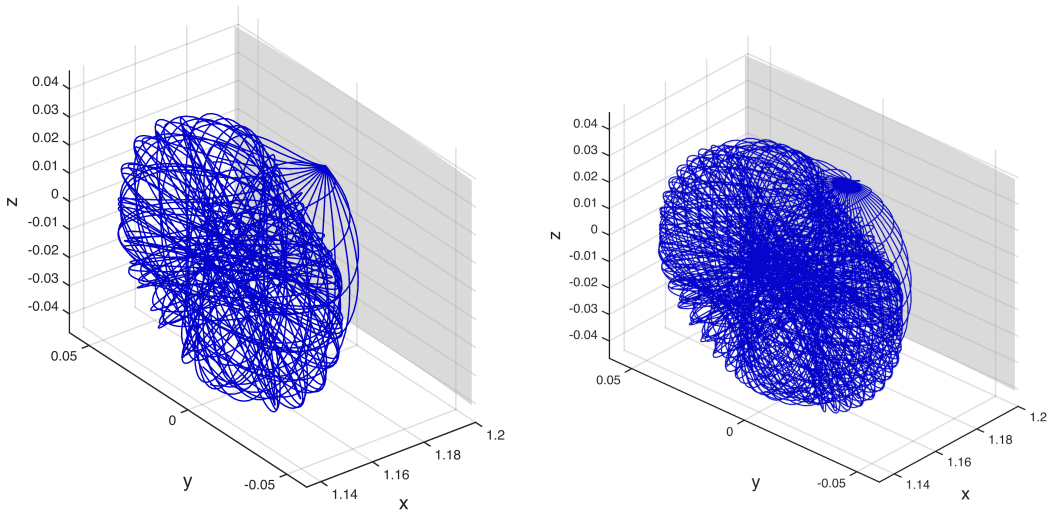

(a) 20 Trajectories (b) 40 Trajectories

Figure 13. Trajectories on W^s of the invariant 3-sphere at C = 3.165 for the point on the cylinder at $\theta = 0.75$ deg. and $z = 0.01$.

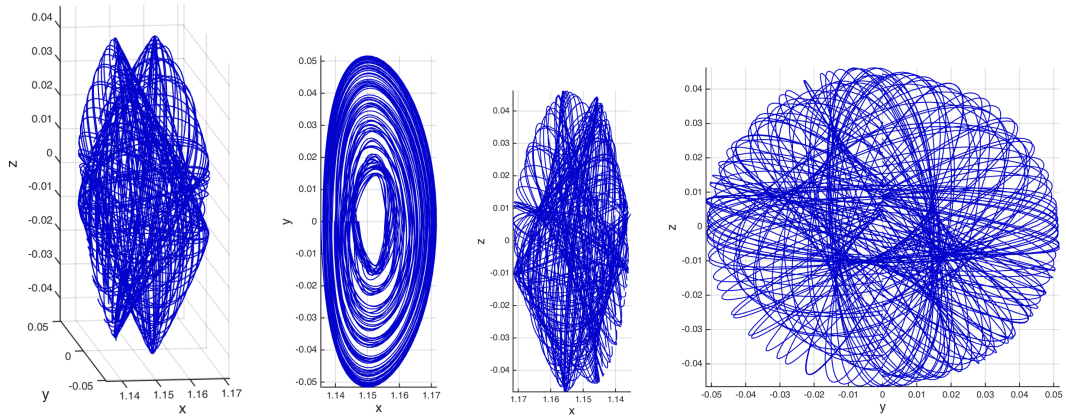

(a) (b) (c) (d)

Figure 14. Asymptotic portion of the trajectories on the invariant 3-sphere W^s approximating the invariant 3-sphere itself.

of initial conditions on the invariant 3-sphere W^s exist. The interior then also contains the transit trajectories, and transit trajectories are constrained to pass through this disk in configuration space.

Comparison with the known Lyapunov orbit W^s

The bisection method clearly captures a range of quasiperiodic motion associated with the invariant 3-sphere at L_2, but the resulting trajectories should also include the W^s of periodic orbits on the invariant 3-sphere. For this to be possible, the point in configuration space should be located at a position that a trajectory on the stable manifold of a periodic orbit passes through. To perform this comparison, a Lyapunov orbit is first computed at C = 3.165, and its corresponding stable manifold is computed using conventional techniques. Trajectories on the Lyapunov orbit W^s are

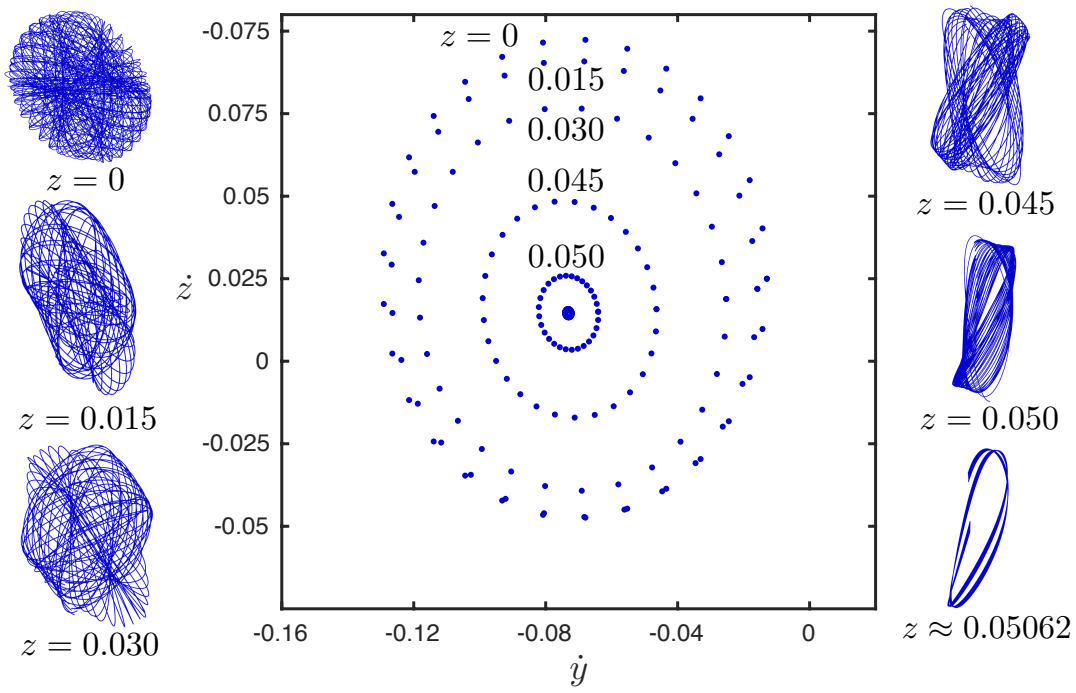

Figure 15. Initial conditions (center) for trajectories on the invariant 3-sphere invariant manifold at selected values of z. The trajectories corresponding to each value of z are shown on the left and right sides. The cases were computed at θ = 0.75 deg. for a Jacobi constant of C = 3.165. The center initial condition point is for $z \approx 0.05062$.

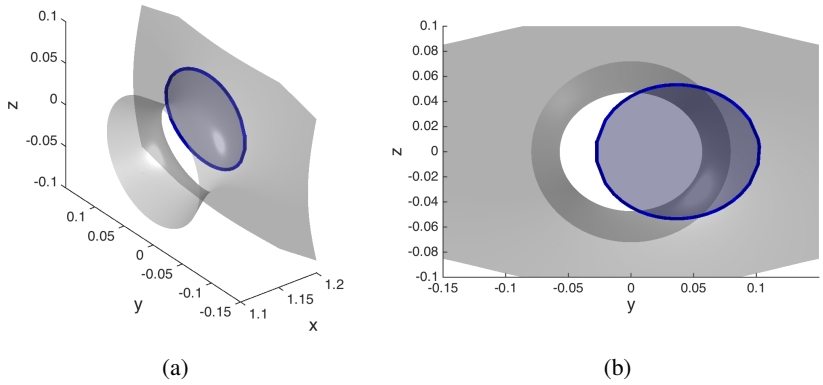

(a) (b)

Figure 16. Border of the invariant 3-sphere W^s in configuration space on the cylinder.

integrated backward in time until they intersect the cylinder at $r = 1.2$ as shown in Figure 17(a). The intersection of one of the stable manifold trajectories with the cylinder was then chosen for the comparison.

Given the selected position in configuration space that has already been shown to intersect with the Lyapunov orbit stable manifold, the bisection method was applied again to the problem, and the initial conditions on the invariant 3-sphere W^s were computed as shown in Figure 17(b). Here, the $\dot{y}$ and $\dot{z}$ values of the Lyapunov W^s computed at this point are shown relative to the invari-

ant 3-sphere W^s initial conditions computed using the bisection method. As can be seen here, the stable manifold trajectory of the periodic Lyapunov orbit is captured as part of the stable manifold of the invariant 3-sphere. Examining the stable manifold point computed using conventional means and the bisection method more closely as seen in Figure 17(b) shows that they differ by less than 7×10^{-13} dimensionless units in velocity. A comparison of the corresponding trajectories in configuration space is also shown in Figure 17. Here, the invariant 3-sphere W^s trajectories are

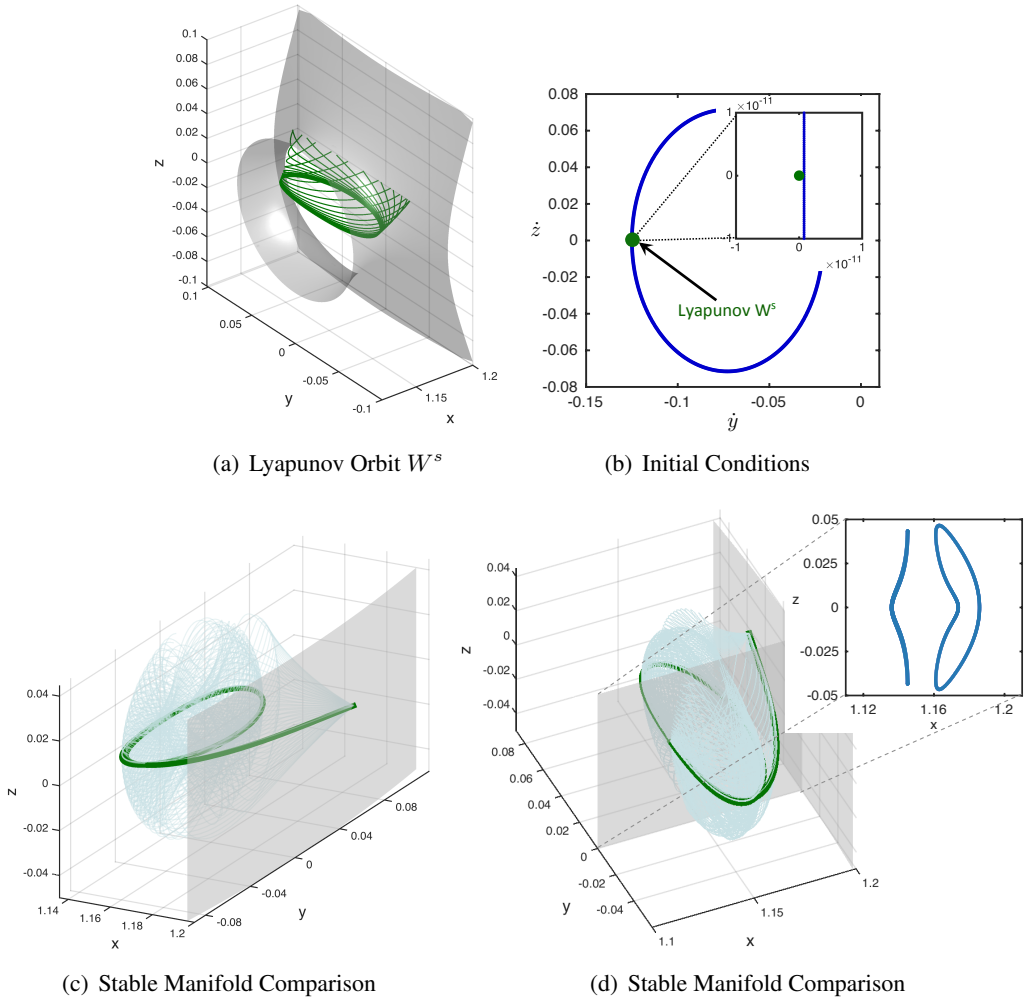

(a) Lyapunov Orbit W^s

(b) Initial Conditions

(c) Stable Manifold Comparison

(d) Stable Manifold Comparison

Figure 17. Lyapunov orbit stable manifold trajectory comparison. The stable manifold of the Lyapunov orbit is shown in green and that of S^3 is shown in blue.

shown in light blue so that the Lyapunov W^s may also be seen. In this case, the other trajectories computed on the invariant 3-sphere W^s range from planar motion to trajectories with a significant z component. While this example focuses on a planar orbit, similar comparisons may be made for three-dimensional periodic orbits as well. Computing the intersections of the final asymptotic portion of the invariant 3-sphere W^s trajectories with a surface of section Σ defined by $y = 0$ can reveal more information about the characteristics of the invariant 3-sphere. Observing the intersections of the trajectory with Σ in configuration space as shown in Figure 17(d), shows two closed curves typical of quasiperiodic orbits or motion on a torus. Further explorations may be made in a similar manner to further understand the characteristics of the invariant 3-sphere.

CONCLUSIONS

A fundamentally new method for computing invariant manifolds using isolating blocks in combination with a bisection method has been successfully applied to the CRTBP at L_2. In particular, the stable and unstable manifolds of Lyapunov orbits near the L_2 energy were computed for the planar CRTBP using this method. In the three-dimensional case, the stable manifold trajectories approaching the invariant 3-sphere at L_2 were computed for a range of positions in configuration space on the isolating block boundary. The bisection method successfully matched the stable manifold velocity for a known location on the stable manifold computed using standard linearization techniques to within 7×10^{-13} dimensionless units. The limits of the transit trajectory locations in configuration space were also quantified, and it was shown that they form a disk. Trajectories on the ω-limit set were approximated using the asymptotic portion of the computed stable manifold trajectories, and both quasiperiodic and periodic motion was observed.

ACKNOWLEDGEMENTS

The research presented here has been carried out at the Jet Propulsion Laboratory, California Institute of Technology, under a contract with the National Aeronautics and Space Administration. This research was funded under the AMMOS/MGSS program. The authors would like to thank Jim Meiss and Holger Dullin for their helpful discussions.

REFERENCES

[1] C. C. Conley, "Notes on the Restricted Three Body Problem: Approximate Behavior of Solutions Near the Collinear Lagrangian Points," Tech. Rep. TMX-53292, NASA, George C. Marshall Space Flight Center, Huntsville, Alabama, 1965.

[2] R. W. Easton, *On the Existence of Invariant Sets Inside a Submanifold Convex to a Flow*. PhD thesis, University of Wisconsin, August 1967.

[3] C. Conley, "Low Energy Transit Orbits in the Restricted Three-Body Problem," *SIAM Journal of Applied Mathematics*, Vol. 16, 1968, pp. 732–746.

[4] R. W. Easton and R. McGehee, "Homoclinic Phenomena for Orbits Doubly Asymptotic to an Invariant Three-Sphere," *Indiana University Mathematics Journal*, Vol. 28, No. 2, 1979, pp. 211–240.

[5] W. S. Koon, M. W. Lo, J. E. Marsden, and S. D. Ross, "Heteroclinic Connections Between Periodic Orbits and Resonance Transitions in Celestial Mechanics," *Chaos*, Vol. 10, June 2000, pp. 427–469.

[6] R. L. Anderson, "Approaching Moons from Resonance via Invariant Manifolds," *Journal of Guidance, Control, and Dynamics*, Vol. 38, June 2015, pp. 1097–1109.

[7] R. L. Anderson and M. W. Lo, "Spatial Approaches to Moons from Resonance Relative to Invariant Manifolds," *Acta Astronautica*, Vol. 105, 2014, pp. 355–372.

[8] Y. Ren and J. Shan, "Numerical Study of the Three-Dimensional Transit Orbits in the Circular Restricted Three-Body Problem," *Celestial Mechanics and Dynamical Astronomy*, October 2012.

[9] J. Llibre, K. R. Meyer, and J. Soler, "Bridges between the Generalized Sitnikov Family and the Lyapunov Family of Periodic Orbits," *Journal of Differential Equations*, Vol. 154, 1999, pp. 140–156.

[10] C. Conley and R. Easton, "Isolated Invariant Sets and Isolating Blocks," *Transactions of the American Mathematical Society*, Vol. 158, July 1971, pp. 35–61.

[11] C. L. Siegel and J. K. Moser, *Lectures on Celestial Mechanics*. Classics in Mathematics, New York: Springer-Verlag, 1971.

[12] K. R. Meyer and G. R. Hall, *Introduction to Hamiltonian Dynamical Systems and the N-Body Problem*. New York: Springer-Verlag, 1992, pp. 109-167.

[13] H. Pollard, *Mathematical Introduction to Celestial Mechanics*. Englewood Cliffs, New Jersey: Prentice-Hall Inc., 1966.

[14] R. W. Easton, *Geometric Methods for Discrete Dynamical Systems*. New York: Oxford University Press, 1998.

[15] R. Moeckel, "Isolating Blocks Near the Collinear Relative Equilibria of the Three-Body Problem," *Transactions of the American Mathematical Society*, Vol. 356, January 2004, pp. 4395–4425.

[16] N. Fenichel, "Persistence and Smoothness of Invariant Manifolds for Flows," *Indiana University Mathematics Journal*, Vol. 21, No. 3, 1971, pp. 193–226.